IET Image Processing

Research Article

IET Journals
The Institution of Engineering and Technology

Vessel transform for automatic optic disk detection in retinal images

ISSN 1751-9659
Received on 4th August 2014
Accepted on 26th February 2015
doi: 10.1049/iet-ipr.2015.0030
www.ietdl.org

Nittaya Muangnak, Pakinee Aimmanee, Stanislav Makhanov ✉, *Bunyarit Uyyanonvara*

Sirindhorn International Institute of Technology, Thammasat University, 131 Moo 5, Tiwanont Road, Bangkadi, Muang, Pathumthani 12000, Thailand
✉ *E-mail: makhanov@siit.tu.ac.th*

Abstract: Precise localisation of an optic disk (OD) in the retinal images is one of the most important problems in the ophthalmic image processing. Although a considerable progress has been made towards a computerised solution of the problem, the numerical algorithms often fail on retinal images characterised by poor quality. Therefore, the authors propose a new method suitable for low-quality images based on exploiting the convergence of the blood vessels to the OD. The novelty of the proposed techniques includes clustering the vessels endowed with a novel correction procedure and the vessel transform (VT) which measures the distance to the main clusters. The algorithm is integrated into the scale-space (SS) analysis to detect the boundary of the OD. The integrated method is called SS algorithm with VT (SSVT). SSVT has been tested on retinal images from two databases with fair and poor images against the fuzzy convergence (FC) method and a modification of the circular transform proposed by Lu. The absolute improvement on sensitivity of SSVT against FC and Lu's are up to 12.37% and 8.18%. Bigger improvements of SSVT in terms of positive predictive value are up to 37.46% and 30.84% against FC and Lu's, respectively.

1 Introduction

Precise automatic localisation of an optic disk (OD) in the retinal images is an important problem in the ophthalmic image processing. Once the OD has been identified, many other regions of clinical importance such as the fovea or macula can be easily detected and/or localised. The OD is also important for establishing a frame of reference within the retinal image. The OD usually appears in the retinal images as a bright, yellowish, circular or oval object, roughly one-sixth the width of the image in diameter [1]. Any irregularity in the appearance of the OD is a sign of abnormalities or diseases such as glaucoma, diabetic retinopathy (DR) or hypertensive retinopathy [2].

Nowadays, one in ten people is advised for annual retinal screening because of a variety of medical conditions [3]. However, annual retinal screening is nearly impossible especially in developing countries because of the huge gap between the number of professional ophthalmologists and the patients. This implies the necessity of automatic screening systems to assist the ophthalmologists in diagnosing the early stage of diseases such as glaucoma and DR using computer-based identification. Since the eye fundus imaging is a frequent clinical procedure, the retinal images are commonly used for a preliminary diagnosis and detecting suspicious cases.

The conventional OD segmentation usually employs a suitable set of features such as brightness, shape, size and the variation of the grey level (entropy) and template matching. Lalonde *et al.* [4] localised the OD by using a pyramidal decomposition based on Haar discrete wavelet transform and segmented the OD using a Hausdorff-based template matching. Li and Chutatape [5] localised the OD by the principal component analysis (PCA) and detected the OD's boundary using an iterative searching procedure called the active shaped model. Lowell *et al.* [6] performed a specialised template matching, and segmentation by using an active contour (snake). Lu *et al.* [3] employed brightness and texture to form a model template. The OD region is determined by a pair of morphological operations and an ellipse is fitted to the detected OD region. Akram and Khan [7] employed the intensity variation and the grey levels as the major features characterising the OD. Curvelet transform has also been applied to solve OD segmentation problem in [8, 9]. Shahbeig and Hossein [10] combined the curvelet transform with the PCA and morphological operators based on geodesic conversions to obtain the OD region. Pereira *et al.* [11] analysed the brightness of a series of blurred images and applied the ant colony optimisation preceded by an anisotropic diffusion filter. Morales *et al.* [12] also used PCA combined with centroid calculation, stochastic watershed and region discrimination. Dehghani *et al.* [13] used histograms of each colour component. Hsiao *et al.* [14] localised the OD by an illumination correction algorithm and segmented the OD contour by using a supervised gradient vector flow snake model. Ramakanth and Babu [15] proposed the OD localisation based on approximate nearest neighbour field. Using the fact that OD appears as a bright region, Pourreza-Shahri *et al.* [16] detected it by using radon transformation of multiple overlapping windows.

One of the most successful works tested against many existing algorithms is Lu [17]. The proposed modification of the circular transform combined with evaluation of the brightness is claimed to be more efficient, more accurate and faster than other state-of-the-art techniques: a morphological approach proposed by Welfer *et al.* [18], a vessel's direction matched filter proposed by Youssif *et al.* [19], localisation using dimensionality reduction of the search space proposed by Mahfouz and Fahmy [20] and genetic algorithms by Carmona *et al.* [21].

The major drawback of the feature-based approaches is that they often incorrectly localise the OD when the OD's physical appearances such as shape, colour, brightness or size become abnormal. The OD obscured by blood vessels or only partially visible (blur, shadows and noise) could be also misclassified. Besides, the feature-based methods could be highly sensitive to distractors which often appear in the retinal images [6].

In the meantime, a powerful subclass of the OD detection algorithms based on the location of the vascular structures is often overlooked. Only a few papers exploit the convergence of the blood vessels to the OD. Akita and Kuga [22] traced the parent–child relationship between blood vessels segments, tracking back

to the centre of the OD. In addition to brightness and shape features of the OD, Chrastek *et al.* [23] checked the area where vertically oriented vessels converge. Foracchia *et al.* [24] used the fact that all retina vessels originate from the OD and their paths follow a similar directional pattern (parabolic course). To describe the general direction of retinal vessels, a geometrical parametric model was proposed, where two of the model parameters are the coordinates of the OD centre. Niemeijer *et al.* [25] approximated the location of the OD using *k*-nearest neighbour regression. Dehghani *et al.* [26] localised the OD by detecting the region having the highest number of vessels, corners and bifurcation points. Welfer *et al.* [27] and Zhang and Zhao [28] used the assumption that the vascular network is alligned horizontally in the retina image. Both work first segmented and skeletonised the network of vessels and checked for the point where the main vessels arcade fragment was intercepted by the horizontal line to obtain the approximated location of OD. The major drawback of this approach is that it is not rotationally invariant. Mendonca *et al.* [29] use the entropy of vascular directions to quantify occurrences and the diversity of vessel orientations of each pixel. Dashtbozorg *et al.* [30] extended this idea using a multi-resolution sliding band filter.

One of the most successful vessel convergence techniques are introduced by Hoover and Goldbaum [1]. The method employing the vessel convergence as the primary feature is based on the fuzzy convergence (FC) endowed with a voting scheme. The voting takes place on the integer grid of the original image. Each vessel is represented by a fuzzy segment, whose area contributes votes to its pixels. The summation of votes at each pixel produces an image map representing the strength of the convergence of each pixel. The map is then blurred and thresholded to produce points of the strongest convergence. The FC techniques have been applied on multiple scales and combined with a feature-based approach employing the equalised brightness. The verification of the method on STructured Analysis of the Retina (STARE) database shows the highest performance overall (89%), and a complete success on the healthy retina test cases (100%). Nonetheless, the method does not consider the hierarchical structure of the vessels and their importance. As a matter of fact, the vessel network consists of the main vessels and several levels of secondary vessels.

The main vessels converge to the OD, whereas the secondary vessels are positioned randomly with regard to the OD. Therefore the vascular network can be thought of as a collection of clusters of connected conduits similar to the river networks. The clusters converge to the OD in the sense that points belonging to the OD are closer to each cluster than points not belonging to OD. This concept is not always true if we consider convergence of individual vessels. It is not hard to give an example where the secondary vessels converge to a false OD.

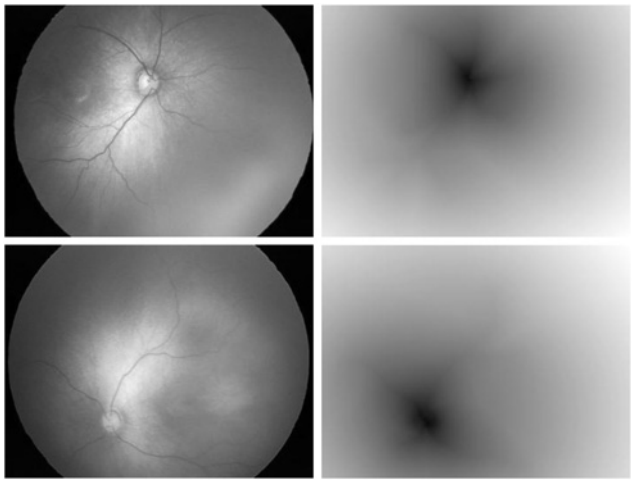

Fig. 1 *Original retinal images (left) and their corresponding VTs (right)*

Therefore we propose new techniques based on clustering of the vessels and a transform which measures the distance to the main vessel clusters. The vessel transform (VT) is generated using a hierarchical clustering combined with a special correction procedure to test the validity of the clusters. The algorithm is integrated into the scale-space (SS) analysis. The new algorithm has been tested on poor quality retinal images from two databases (172 images) against the FC method [1], and a recent modification of the circular transform [17]. Furthermore, the space scale boundary detection [31] was tested with and without the VT option. The numerical experiments demonstrate that the proposed algorithm outperforms the benchmark methods in terms of the correct localisation of the OD and improves segmentation of the OD based on the space scale scheme.

2 Vessel transform

The VT is given by

$$V(p) = \frac{1}{N}\sum_{i=1}^{N} \mathrm{dist}(p,\ c_i) \tag{1}$$

where c_i is the i^{th} cluster of vessels, N is the number of clusters, $p = (x,\ y)$ is an arbitrary point in the image and $\mathrm{dist}(p,\ c) = \min_{p' \in c} ||p - p'||$. An introductory example in Fig. 1 displays sample retinal images and the corresponding VTs. The dark part of the VT image corresponding to the vessel convergence region locates the OD.

Clearly, our approach requires a reliable and accurate vessel segmentation method. At the moment, there exist numerous vessel segmentation algorithms applicable to variety of retinal images [32–35]. Our numerical experiments with available source codes revealed a good performance of the automated retinal image analyser [35, 36] developed by the Centre for Vision and Vascular Science of Queen's University of Belfast. The method is based on thresholding of wavelet coefficients on different spatial scales and vessel location refinement using the centreline spline fitting. The method is unsupervised and does not use any masks or filters since they often must be tailored for a particular type or resolution of image and require modifications to be applied to others. As opposed to that the choice of wavelet levels and thresholds does not need to be changed for similar images. Following [35, 36], we set the wavelet coefficients threshold to identify the lowest 20% of coefficients as vessels. Although this typically produces an oversegmented image, small isolated objects and holes inside the vessels can be easily removed by morphological operations.

The input of the clustering algorithm is a collection of vessels (v_1, v_2, …, v_m). Each vessel is represented by the Cartesian coordinates: $v_i = ((x,\ y)_{i,1},\ (x,\ y)_{i,2},\ \ldots,\ (x,\ y)_{i,N_i})$. The first step is pre-processing designed to remove the outliers: short, thin and faint vessels. It requires the following thresholds: T_{l} is the length threshold, T_{t} is the thickness threshold, T_f is the threshold on the grey-level intensity of the vessel relative to the background. The second step merges the vessels into clusters and removes the isolated vessels. The merging step employs a threshold T_{d} on the maximum distance between clusters which can be merged into a new cluster. We apply a classical hierarchical bottom-up clustering endowed with an original correction procedure. Initially, the algorithm treats each vessel as a singleton $c_i = v_i$. Next, it successively merges clusters c_i, c_j if $\mathrm{dist}(c_i,\ c_j) < T_{\mathrm{d}}$ until they have been merged into several well separated sets. The post-processing procedure detects and removes the outliers (small clusters) by using the condition $N_{c_i} < T_L$, where N_{c_i} denotes the size of the cluster and T_L denotes the corresponding threshold.

Note that clustering does not include time-consuming tracing procedures designed to detect the tree-like structures of the vessels. However, if trained, the algorithm returns well separated clusters sufficient to generate a VT which localises the

IET Image Process., 2015, Vol. 9, Iss. 9, pp. 743–750

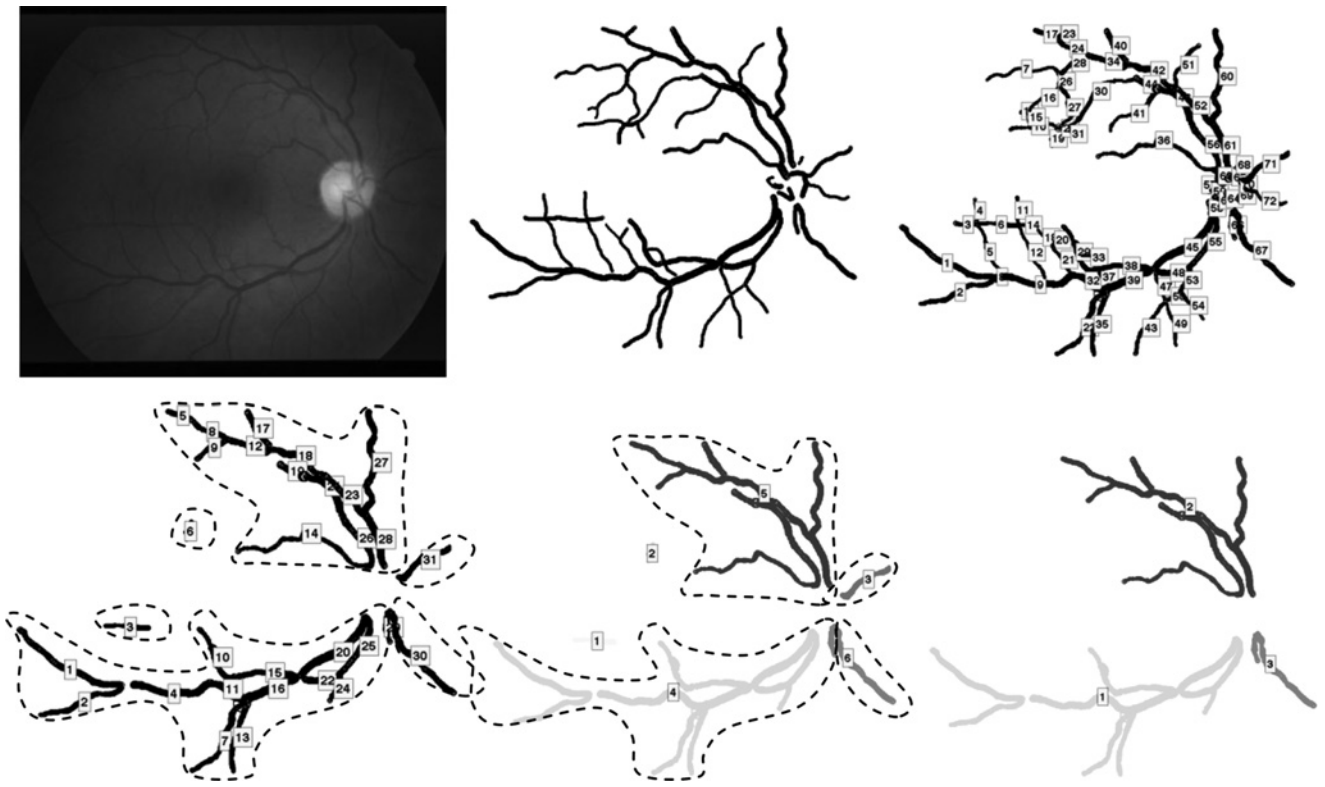

Fig. 2 *Original image (top left), extracted vessels (top middle), segmented vessels (top right), removing short, thin and faint vessels (bottom left), removing small clusters (bottom middle), final clusters (bottom right)*

convergence region and consequently the OD. Fig. 2 illustrates the proposed clustering method.

3 Correction algorithm

The VT-based segmentation of the OD requires that the resulting clusters converge to the OD. Therefore for the vessel networks separated into three or more clusters, we verify the quality of convergence as follows. First, we evaluate the convergence region $\Omega = \arg\min_p V(p)$ and its centroid. Next, we withdraw the clusters one by one from the collection and evaluate the convergence regions Ω' corresponding to these new collections. If for some Ω′, $\text{dist}(O_\Omega, O_{\Omega'}) > T_\Omega$, where O_Ω is the centroid of Ω, O'_Ω is the centroid of Ω′ and T_Ω is the corresponding threshold, the clustering is discarded. Our assumption is that if the vessels strongly converge to Ω, the system without one cluster converges approximately to the same region (see Fig. 3).

Furthermore, if $\min_{c_i}(\text{dist}(c_i, \Omega_c)) < T_{VT}$, where T_{VT} is the corresponding threshold and c_i is the i^{th} cluster and Ω_c is the centroid of Ω (the cluster is close enough to the convergence region), the clustering is considered successful. In this case, the VT is included in the prescribed set of features for a further evaluation.

4 Threshold selection

The proposed method requires the following thresholds: T_l is the minimal acceptable length of the vessel for a particular image (shorter vessels will be eliminated), T_t is the minimal acceptable thickness, T_f is the maximum acceptable intensity of the vessel relative to the background, T_d is the maximum distance between the clusters which can be merged into a new cluster, T_L is the minimum acceptable size of the cluster and T_Ω, T_{VT} used by the convergence test (see Section 3). The thresholds are obtained using a bivariate quadratic approximation given by

$$T(\mu, \sigma) = a_1\mu^2 + a_2\sigma^2 + a_3\mu + a_4\sigma + a_5\mu\sigma + a_6 \quad (2)$$

where μ and σ are the mean and the standard deviation of the corresponding parameter evaluated for a particular image. For instance, $T_l \equiv T_l(\mu_l, \sigma_l)$ is the threshold on the minimal acceptable length of the vessel, whereas μ_l is the mean length of a vessel in a particular image and σ_l is the standard deviation (see Fig. 7).

5 SS algorithm with VT

The VT method with the improvements described in Sections 2–4 generated an approximated location of the OD but it has not yet detected the boundary of the OD. To obtain the OD's rim, we

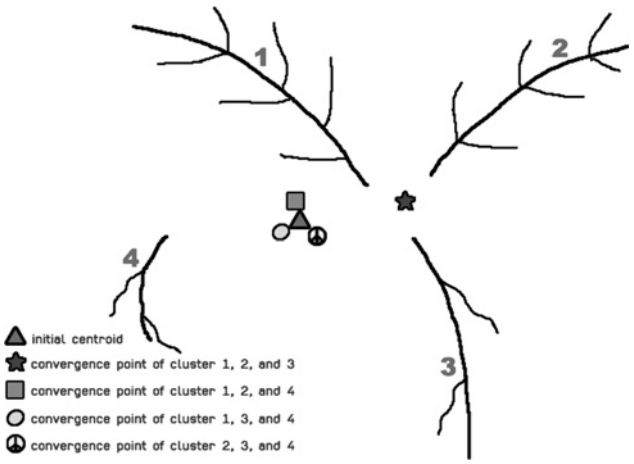

Fig. 3 *Convergence test*

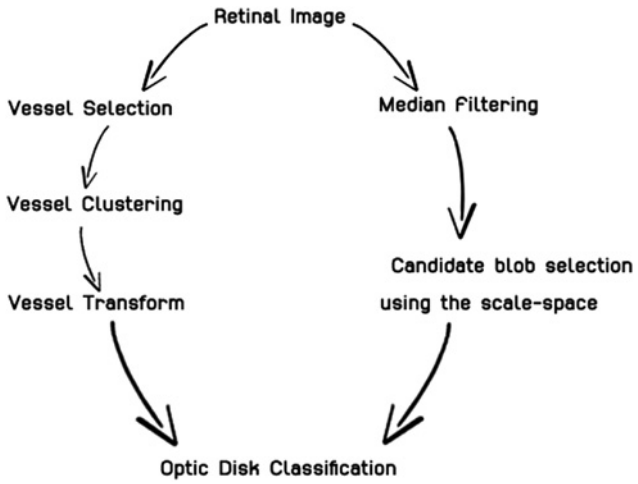

Fig. 4 *VT combined with the SS segmentation*

integrate our approach into the SS boundary detection algorithm proposed by Duanggate *et al.* [31]. The modified algorithm is called the space scale algorithm with the VT (SSVT). Fig. 4 shows the proposed integration of SS and VT into the SSVT.

The SS approach is based on the original theory proposed by Lindeberg [37] in 1994. The image is converted into a one-parameter family of smoothed images. Objects (blobs) which appear stable under smoothing at different scales along with their features such as the size, the compactness, the entropy, the average intensity etc. are considered as the OD candidates. We modify the SS algorithm by adding the VT score as an additional feature. To integrate the feature in the SS method, we use an automatic decision tree generator available from the Waikato Environment for Knowledge Analysis [38]. The examples of the decision trees are given in Section 7.

6 Experimental setup

We tested the proposed method against the existing techniques on two collections of images, that is, the STARE [39] which is a standard collection available on the internet and a dataset originally collected to detect the signs of retinopathy of prematurity (ROP) by Dr. Sarah Barman with Kingston University of UK. All digital retinal images from ROP were taken from patients with non-dilated pupils using a KOWA-7 non-mydriatic retinal camera with a 45° field of view. The images were stored in JPEG format 640 × 480 pixels at 24 bits per pixel.

To reduce the inconsistency between human experts, the ground truth was obtained from three ophthalmologists from Thammasat University Hospital, Thailand. The ophthalmologists were asked to hand-draw the OD rims on each retina image from two collections three times. To check the inter-observer variability and intra-observer variability, we used the voting overlapping score defined as the ratio of an area in the image that at least two ground truths agree on that it is part of OD to the area obtained from the union of the three ground truth contours. The inter-observer variability values of the experts are 0.86 and 0.91 for the ROP and STARE collections, respectively. The intra-observer variabilities of each expert are 0.92 and 0.93 on average for the ROP and STARE collections, respectively.

Images with bright, round and clear border of the ODs were classified visually as 'fair', the rest is considered 'poor'. There are 60 images with fair quality and 31 images with poor quality for the ROP collection, whereas 31 images with fair quality and 50 images with poor quality for the STARE collection. Figs. 5*a* and 5*b* display examples of 'fair' and 'poor' images.

Our two collections of test images have been obtained by different devices with different lighting conditions. Therefore, they require different sets of thresholds which are obtained by the quadratic regression (2). Fig. 6 illustrates the proposed threshold selection. We train the method using the classic 70–30% ratio between the training and the testing data.

To combine features in SS method, we use an automatic decision tree generation available from the Waikato Environment for Knowledge Analysis [38]. Features evaluated for the candidate blob in scaled space are the size (s), the compactness (c), the entropy (e), the average intensity (i) and the average value of the VT (V). The resulting decision trees and the particular thresholds are shown in Fig. 7.

Note that the decision trees indicate the importance of V, s and c, whereas the branches including the entropy and the intensity have been automatically pruned. The forthcoming Section 7 shows how the VT improves the accuracy of the classification.

7 Experiments and results

In this section, we show and analyse results of applying the proposed algorithm to the ROP and STARE collections of retinal images. We

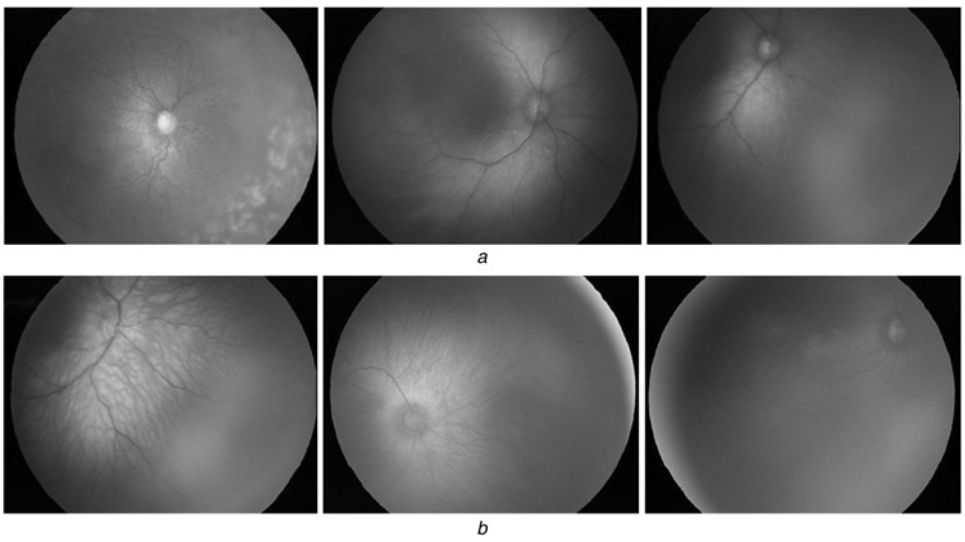

Fig. 5 *Examples of the 'fair' and the 'poor' images*

a Fair images
b Poor images

IET Image Process., 2015, Vol. 9, Iss. 9, pp. 743–750

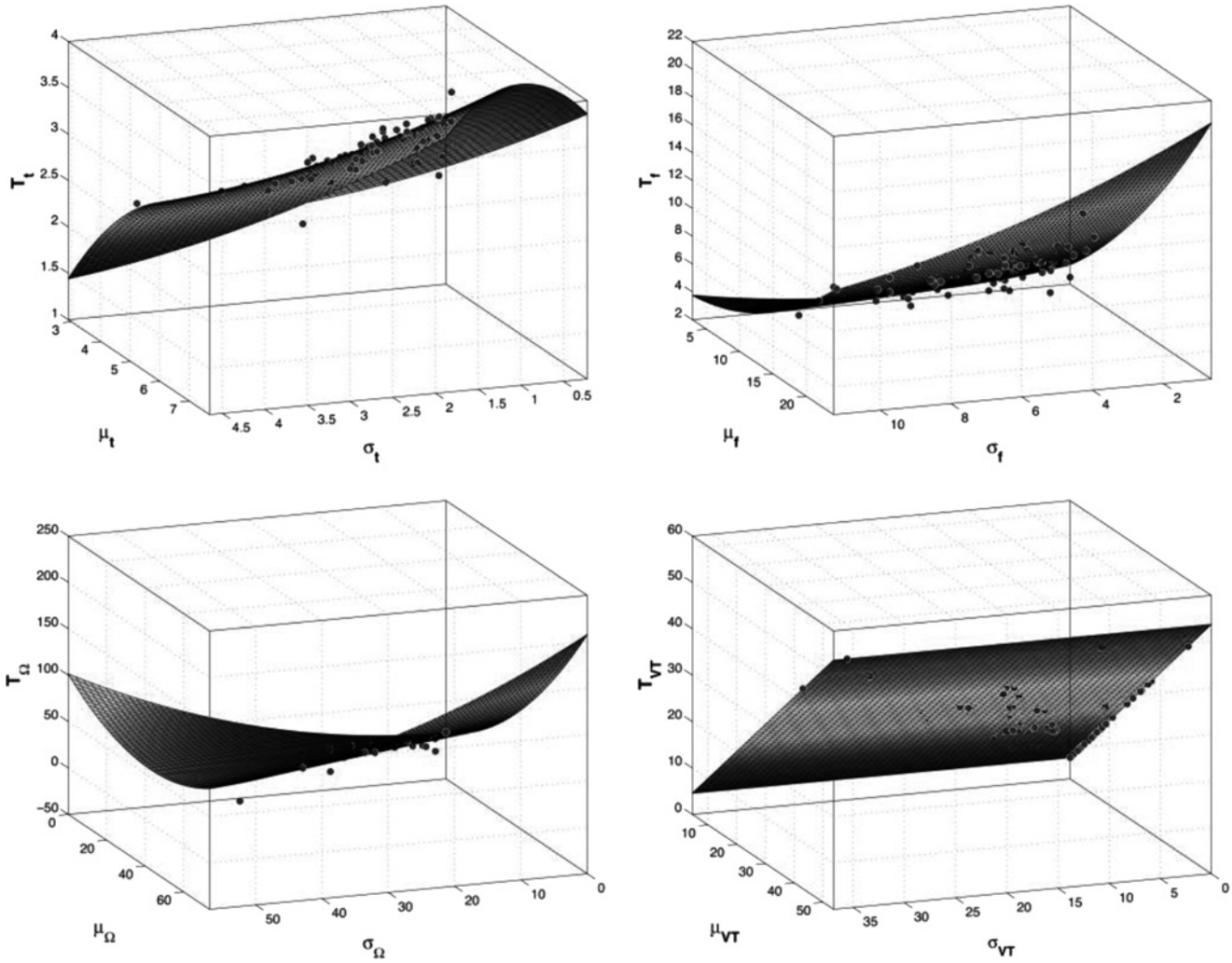

Fig. 6 *Example of quadratic regression applied to the STARE collection*

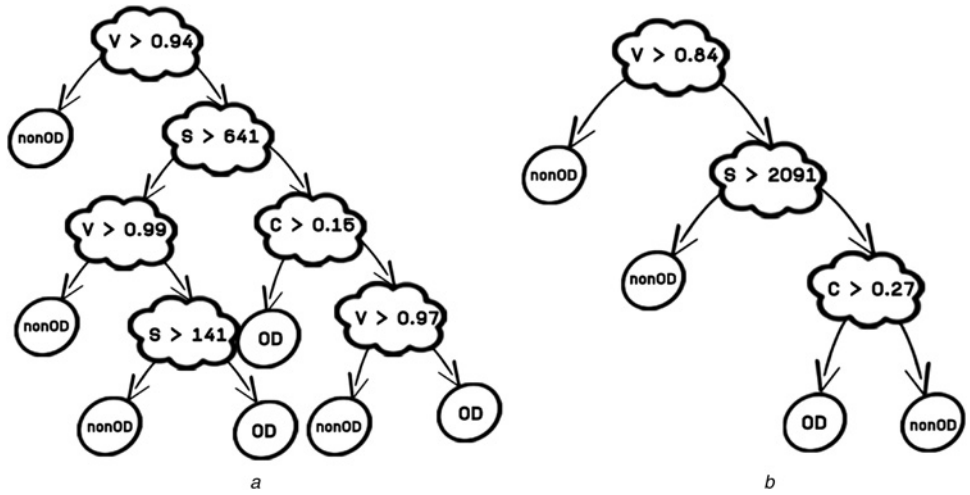

Fig. 7 *Decision trees for test collections*

a ROP collection
b STARE collection

test the method against FC method [40] and a recent modification of the circular transform proposed in [17]. Furthermore, we compare the standard SS segmentation [31] and the SS method endowed with the proposed VT.

7.1 Performance of the VT in locating the OD

We applied and compared the performance of VT with the advanced version of the circular transform Lu's method [17] and FC method [1]. Fig. 8 shows introductory examples when Lu's method or/and

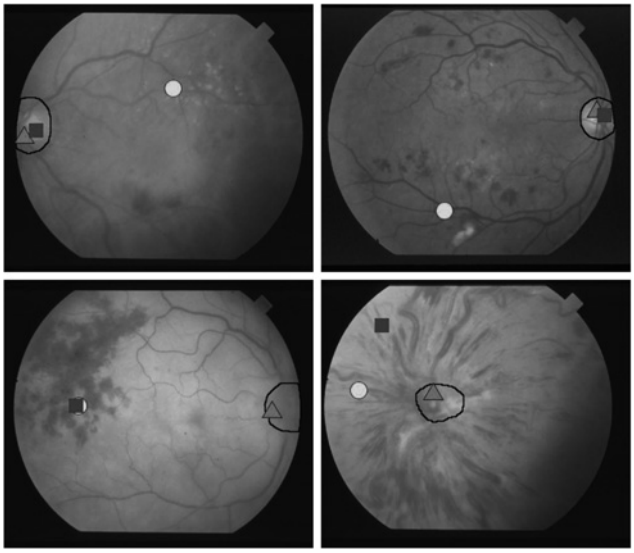

Fig. 8 *OD location: ground truth – solid line, VT – triangle, FC – circle and Lu's – square*

FC fail, whereas the proposed method indicates the correct OD location.

The accuracy of the OD locating was evaluated as follows. If the convergence region Ω (see Section 3) is contained entirely inside the ground truth contour, we consider it a correct location of the OD. Lu's method was considered successful if the centroid of the circular transform contour was located inside the ground truth contour.

Table 1 shows the accuracy of the location of the OD location for the fair and poor images processed by the VT, FC and Lu on the STARE collection. The VT outperforms FC for both the groups with the absolute improvement of about 6%. However, Lu's method is slightly better. This is because of the better quality of the images in that database. However, the VT performs much better on fair and poor quality images from ROP database as follows: fair images: Lu's-88%, VT-95% and poor images: Lu's-64.5%, VT-96.7%.

Furthermore, the advanced circular transform of Lu claims to be the fastest and the most accurate as compared with line operator method [18], geometrical model method [19], the vessel direction matched filter [20] and the dimensionality reduction method [21]. Therefore we conjecture that our proposed algorithm should outperform the above-mentioned procedures for the poor images as well.

7.2 Performance of the SSVT in detecting the OD region

Next, we combine our approach with the SS algorithm for detecting the OD proposed by Duanggate *et al.* [31]. We extend the SS algorithm by adding the VT score as an additional feature. The modified algorithm is called the SSVT. Our OD classification is performed using a decision tree which includes the above-mentioned features along with the VT-feature. As opposed to the previous section where the location of the OD was evaluated by finding the centroid of the convergence area, the OD region is now determined by using a combination of the SS which generates the candidate blobs and the proposed decision tree (Fig. 7).

We evaluate the performance using two standard schemes: sensitivity and positive predictive value (PPV). The first one reveals the accuracy while the second one reflects completeness of the obtained solution. The sensitivity is defined to be the ratio of the number of pixels detected correctly as OD to the total number of pixels detected as OD. The PPV is the ratio of number of pixels detected correctly as OD to the total number of pixels of OD from the ground truth.

The algorithms were tested on the ROP and the STARE collections. Fig. 8 shows examples when SSVT outperforms the other two approaches. The VT-feature has a strong impact on the blob classification process. In many cases, the SS and Lu fail to detect the OD because of insufficient information provided by the basic features. As opposed to that, SSVT employs the convergence of the vessels which is not sensitive to the variation of the contrast and the noise as long as the entire vascular network or at least a major part of it has been correctly detected and clustered.

The tests of the performance of the SSVT against the SS and Lu's are presented in Table 2. The bold values represent the best result in a particular category. The SSVT outperforms SS and Lu's in 'both quality measures for each group of the images (fair and poor) and for each collection of data'. In particular, when the image quality is poor, the SSVT outperforms the other two approaches in terms of PPV considerably (Table 3).

For the fair images, the advantages of the SSVT over SS in average sensitivity are up to 2.09% (STARE) and 4.45% (ROP). The SSVT underperforms Lu's in average sensitivity by 10.19% (STARE) but outperforms Lu's by 8.18%. For the poor images,

Table 1 Accuracy of the OD location

Collections	Image quality	Accuracy, %			Absolute improvement VT against FC, %	Absolute improvement VT against Lu's, %
		FC	VT	Lu's		
ROP	fair	N/A	95	88.33	N/A	6.68
	poor	N/A	96.77	64.52	N/A	32.25
STARE	fair	90.32	96.77	100	6.45	–3.23
	poor	88	94	98	6	–4
average (STARE only)		89.16	95.39	98.77	6.23	–3.38
average (ROP only)		N/A	95.89	76.42	N/A	19.47

VT against FC and Lu's circular transform.

Table 2 Average sensitivity and PPV of SS and Lu's against SSVT

Collections	Image quality	Average sensitivity			Average PPV		
		Lu's	SS	SSVT (SSVT-Lu's, SSVT-SS)	Lu's	SS	SSVT (SSVT-Lu's, SSVT-SS)
ROP	fair	74.29	80.39	**82.47** (+8.18, +2.08)	66.42	86.08	**87.41** (20.99, 1.33)
	poor	**61.28**	45.51	58.18 (–3.1, 12.67)	46.39	53.01	**83.85** (37.46, 30.84)
STARE	fair	**72.59**	57.95	62.4 (–10.19, 4.45)	**84.66**	67.09	74.14 (–10.52, 7.05)
	poor	41.23	43.27	**45.76** (4.53, 2.49)	69.89	59.18	**74.59** (4.7, 15.41)
average		62.35	62.2	**64.26** (1.91, 2.06)	66.84	66.34	**80** (13.16, 13.66)

IET Image Process., 2015, Vol. 9, Iss. 9, pp. 743–750

Table 3 Computational time Lu's against SSVT

Percentage of test pixels, %	Number of radial line segments	Average time Lu's, min	Average time SSVT, min
20	40	1.57	4.85
20	180	6.63	
60	40	4.29	
60	180	18.84	

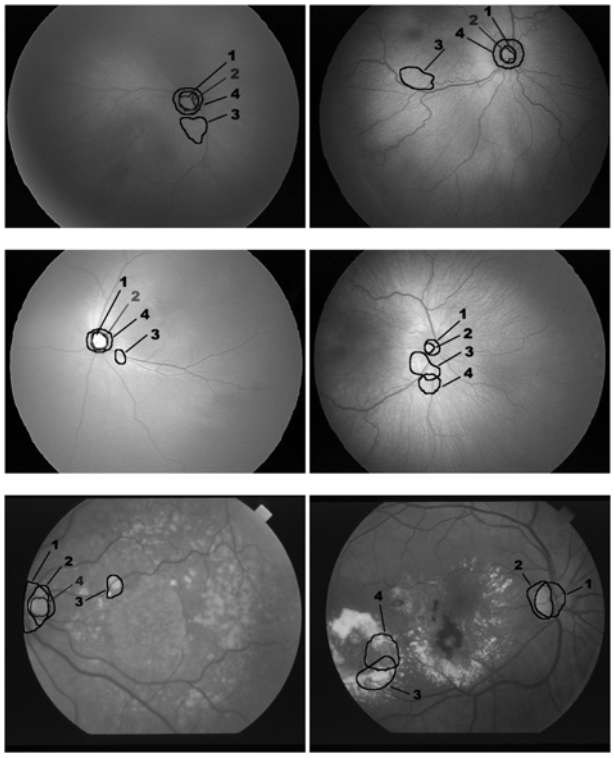

Fig. 9 *Examples of the OD segmentation, 1-ground truth, 2-SSVT, 3-SS, 4-Lu's*

the SSVT outperforms SS by 2.49% (STARE) and 12.67% (ROP). The SSVT outperforms Lu's in average sensitivity by 4.53% (STARE) but underperforms Lu's slightly by 3.1%.

A good improvement of the SSVT over SS and Lu's is notable from the PPV results on the ROP collection. For the fair group of the ROP collection, SSVT outperforms SS by 1.33% and LU's by 20.99%, whereas bigger improvements obtained for the poor group of the same collection, SSVT outperforms SS by 30.84% and Lu's by 37.46%. For the fair group of the STARE collection, SSVT outperformed SS by 7.05% but underperformed SS by 10.52%. For the poor group of STARE collection, SSVT outperformed SS and Lu's by 15.41 and 4.7%, respectively (see Fig. 9).

It should be noted that in [31] SS was found to be superior with regard to the OD segmentations based on the morphological operations [41] and the circular Hough transform applied to ROP [40]. Moreover, in [17] Lu's claimed to outperform methods [18–21]. Therefore the SSVT outperforms the above-mentioned methods as well with a greater advantage. Still there are images where SSVT fails. Those images are usually characterised by unclear vascular networks combined with noise and shadows shaped similarly to the vessels.

Furthermore, although Lu's method is claimed to be the fastest, actually, its performance strongly depends on the threshold on the grey level to select possible candidates for the centre of the OD and the number of radial segments used to verify the circularity of the object boundary. Lu also claims that the centre of the OD 'nearly always lies within the first 20% brightest pixels within the OD probability map'. However, there are many images for which it is not correct. In turn, increasing this threshold, increases the computational time. For instance, changing the threshold from 20 to 60% doubles it. In turn, changing the angular step between the required radial segments from 6° to 2° increases the computational time of Lu's by a factor of 10. As opposed to that the computational time of the proposed method does not depend on the thresholds. Our method has been programmed in MATLAB and requires about 4 minutes to process a standard database image 600×800 on a Dell computer with 3.30 GHz Intel Core i3 Processor and 4 GB of random access memory.

The improved accuracy of the proposed algorithm applied to the poor quality images makes it possible to suggest a switch from the circular transform-based methods to VT scheme when the quality of the OD boundary is poor.

8 Limitations of the method

In some cases, the clustering algorithm returns an unacceptable result which includes only one or two clusters. In this case, we could not reliably test the convergence. Technically, one can modify the thresholds and merge the vessels into a new set of clusters. However, an algorithm based on this idea is still an open problem. In this case, following [31] we simply discard the VT-feature and apply the SS algorithm in its original version [37]. The numerical experiments show that the number of the images characterised by poor convergence usually does not exceed 10%.

The algorithm requires a good quality of the vessel segmentation in the sense of strong convergence of the vessel network to the OD (see Section 3). In case of poor convergence, the algorithm must automatically recognise this and switch to the OD detection based on other features such as the intensity and compactness (the circular transform). Finally, the algorithm includes seven thresholds which require training and construction of the decision trees. The thresholds could be different for different datasets.

9 Conclusions

The proposed new VT improves the accuracy of locating the OD. The combination of the VT with the feature-based SS segmentation improves the quality of the OD segmentation. The absolute improvement of the SSVT over SS measured in terms of sensitivity and PPV is approximately 14% and 30%. Respectively the improvement in approximating the location of the OD is up to 32%. In addition, the absolute improvement of the SSVT over Lu's method measured in terms of sensitivity and PPV is approximately 8% and 37.46%. However, such an improvement can be achieved given a good segmentation of the vessels and when the vessel network strongly converges to the OD.

10 Acknowledgments

The authors gratefully acknowledge grant number RSA5780034 of Thailand Research Fund and Center of Excellence in Biomedical Engineering of Thammasat University for the financial support. We also wish to thank Department of Ophthalmology, Faculty of Medicine, Thammasat University for the ground truth and variability tests.

11 References

1 Hoover, A., Goldbaum, M.: 'Locating the optic nerve in a retinal image using the fuzzy convergence of the blood vessels', *IEEE Trans. Med. Imaging*, 2003, **22**, (8), pp. 951–958

2 Li, H., Chutatape, O.: 'Automated feature extraction in color retinal images by a model based approach', *IEEE Trans. Biomed. Eng.*, 2004, **51**, (2), pp. 246–254

3 Lu, S., Liu, J., Lim, J.H., *et al.*: 'Automatic optic disc segmentation based on image brightness and contrast'. SPIE Medical Imaging, Int. Society for Optics and Photonics, 2010, vol. 76234J, pp. 1–8

4 Lalonde, M., Beaulieu, M., Gagnon, L.: 'Fast and robust optic disc detection using pyramidal decomposition and Hausdorff-based template matching', *IEEE Trans. Med. Imaging*, 2001, **20**, (11), pp. 1193–1200
5 Li, H., Chutatape, O.: 'Boundary detection of optic disk by a modified ASM method', *Pattern Recognit.*, 2003, **36**, (9), pp. 2093–2104
6 Lowell, J., Hunter, A., Steel, D., *et al.*: 'Optic nerve head segmentation', *IEEE Trans. Med. Imaging*, 2004, **23**, (2), pp. 256–264
7 Akram, U.M., Khan, S.A.: 'Automated detection of dark and bright lesions in retinal images for early detection of diabetic retinopathy', *J. Med. Syst.*, 2012, **36**, pp. 3151–3162
8 Esmaeili, M., Rabbani, H., Dehnavi, A.M., Dehghani, A.: 'Automatic detection of exudates and optic disk in retinal images using curvelet transform', *IET Image Process.*, 2012, **6**, (7), pp. 1005–1013
9 Esmaeili, M., Rabbani, H., Dehnavi, A.M.: 'Automatic optic disk boundary extraction by the use of curvelet transform and deformable variational level set model', *Pattern Recognit.*, 2012, **45**, pp. 2832–2842
10 Shahbeig, S., Hossein, P.: 'Fast and automatic algorithm for optic disc extraction in retinal images using principle-component-analysis-based preprocessing and curvelet transform', *J. Opt. Soc. Am.*, 2013, **30**, pp. 13–21
11 Pereira, C., Goncalves, L., Ferreira, M.: 'Optic disc detection in color fundus images using ant colony optimization', *Med. Biol. Eng. Comput.*, 2013, **51**, pp. 295–303
12 Morales, S., Naranjo, V., Angulo, J., Alcaniz, M.: 'Automatic detection of optic disc based on PCA and mathematical morphology', *IEEE Trans. Med. Imaging*, 2013, **32**, (4), pp. 786–796
13 Dehghani, A., Moghaddam, H.A., Moin, M.S.: 'Optic disc localization in retinal images using histogram matching', *EURASIP J. Image Video Process.*, 2012, **19**, pp. 1–13
14 Hsiao, H.K., Liu, C.C., Yu, C.Y., Kuo, S.W., Yu, S.S.: 'A novel optic disc detection scheme on retinal images', *Expert Syst. Appl.*, 2012, **39**, pp. 10 600–10p 606
15 Ramakanth, S.A., Babu, R.V.: 'Approximate nearest neighbor field based optic disk detection', *Comput. Med. Imaging Graph.*, 2014, **38**, pp. 49–56
16 Pourreza-Shahri, R., Tavakoli, M., Kehtarnavaz, N.: 'Computationally efficient optic nerve head detection in retinal fundus images', *Biomed. Signal Process. Control*, 2014, **11**, pp. 63–73
17 Lu, S.: 'Accurate and efficient optic disc detection and segmentation by a circular transformation', *IEEE Trans. Med. Imaging*, 2011, **30**, (12), pp. 2126–2133
18 Welfer, D., Scharcanski, J., Marinho, D.: 'A morphologic two-stage approach for automated optic disk detection in color eye fundus images', *Pattern Recognit. Lett.*, 2013, **34**, (5), pp. 476–485
19 Youssif, A., Ghalwash, A.Z., Ghoneim, A.: 'Optic disc detection from normalized digital fundus images by means of a vessels' direction matched filter', *IEEE Trans. Med. Imaging*, 2008, **27**, pp. 11–18
20 Mahfouz, A.E., Fahmy, A.S.: 'Ultrafast localization of the optic disc using dimensionality reduction of the search space', *Med. Image Comput. Comput. Assist. Interv.*, 2009, **5762**, pp. 985–992
21 Carmona, E.J., Rincon, M., Garcia-Feijoo, J., Martinez-de-la-Casa, J.M.: 'Identification of the optic nerve head with genetic algorithms', *Artif. Intell. Med.*, 2008, **43**, pp. 243–259
22 Akita, K., Kuga, H.: 'A computer method of understanding ocular fundus images', *Pattern Recognit.*, 1982, **15**, (6), pp. 431–443
23 Chrastek, R., Skokan, M., Kubecka, L., *et al.*: 'Multimodal retinal image registration for optic disk segmentation', *Methods Inf. Med.*, 2004, **43**, (4), pp. 336–342
24 Foracchia, M., Grisan, E., Ruggeri, A.: 'Detection of optic disc in retinal images by means of a geometrical model of vessel structure', *IEEE Trans. Med. Imaging*, 2004, **23**, (10), pp. 1189–1195
25 Niemeijer, M., Abràmoff, M.D., van Ginneken, B.: 'Fast detection of the optic disc and fovea in color fundus photographs', *Med. Image Anal.*, 2009, **13**, (6), pp. 859–870
26 Dehghani, A., Moin, M.S., Saghafi, M.: 'Localization of the optic disc center in retinal images based on the Harris corner detector', *Biomed. Eng. Lett.*, 2012, **2**, (3), pp. 198–206
27 Welfer, D., Scharcanski, J., Kitamura, C., Pizzol, M., Ludwig, L., Marinho, D.: 'Segmentation of the optic disk in color eye fundus images using an adaptive morphological approach', *Comput. Biol. Med.*, 2010, **40**, (2), pp. 124–137
28 Zhang, D., Zhao, Y.: 'Novel accurate and fast optic disc detection in retinal images with vessel distribution and directional characteristics', *IEEE J. Biomed. Health Inf.*, 2013, **PP**, pp.1–10
29 Mendonca, A.M., Sousa, A., Mendonca, L., Campilho, A.: 'Automatic localization of the optic disc by combining vascular and intensity information', *Comput. Med. Imaging Graph.*, 2013, **37**, pp. 409–417
30 Dashtbozorg, B., Mendonca, A.M., Campilho, A.: 'Optic disc segmentation using the sliding band filter', *Comput. Biol. Med.*, 2015, **56**, pp. 1–12
31 Duanggate, C., Uyyanonvara, B., Makhanov, S.S., Barman, S., Williamson, T.: 'Parameter-free optic disc detection', *Comput. Med. Imaging Graph.*, 2011, **35**, pp. 51–63
32 Fraz, M.M., Remagnino, P., Hoppe, A., *et al.*: 'Blood vessel segmentation methodologies in retinal images – a survey', *Comput. Methods Programs Biomed.*, 2015, **56**, (1), pp. 407–433
33 Uyen Nguyen, T.V., Bhuiyan, A., Laurence Park, A.F., Ramamohanarao, K.: 'An effective retinal blood vessel segmentation method using multi-scale line detection', *Pattern Recognit.*, 2013, **46**, (3), pp. 703–715
34 Badsha, S., Reza, A.W., Tan, K.G., Dimyati, K.: 'A new blood vessel extraction technique using edge enhancement and object classification', *J. Digit. Imaging*, 2013, **26**, (6), pp. 1107–1115
35 Bankhead, P., Scholfield, C.N., McGeown, J.G., Curtis, T.M.: 'Fast retinal vessel detection and measurement using wavelets and edge location refinement', *PLoS ONE*, 2012, **7**, (3), pp. 1–12(e32435)
36 ARIA: 'Retinal vessel detection using MATLAB'. Available at http://www.sourceforge.net/p/aria-vessels, Retrieved 24 October 2012
37 Lindeberg, T.: 'Scale-space theory in computer vision' (Kluwer Academic Publishers, Netherlands, 1994)
38 Hall, M., Frank, E., Holmes, G., Pfahringer, B., Reutemann, P., Witten, I.H.: 'The WEKA data mining software: an update'. SIGKDD Explorations, 2009, vol. 11, no. 1, pp. 10–18
39 Hoover, A.: 'The structure analysis of the retina (STARE) project (website)'. Available at http://www.ces.clemson.edu/~ahoover/stare, Retrieved 18 February 2013
40 Sekhar, S., Al-Nuaimy, W., Nandi, A.K.: 'Automated localisation of retinal optic disk using Hough transform'. Fifth IEEE Int. Symp. Biomedical Imaging: From Nano to Macro, 2008, pp. 1577–1580
41 Sopharak, A., Uyyanonvara, B., Barman, S., Williamson, T.H.: 'Automatic detection of diabetic retinopathy exudates from non-dilated retinal images using mathematical morphology methods', *Comput. Med. Imaging Graph.*, 2008, **32–8**, pp. 720–727